Tellus (1986), *38A*, 60–75

Numerical study of some neutrally and unstably stratified boundary-layer flows over a valley at small Richardson number

By J. D. CARLSON[1], *Atmospheric Sciences Program* and M. R. FOSTER, *Department of Aeronautical and Astronautical Engineering, The Ohio State University, Columbus, Ohio 43210, USA*

(Manuscript received August 27, 1984; in final form March 22, 1985)

ABSTRACT

A two-dimensional numerical model is utilized to investigate steady-state, three-dimensional turbulent flow over a valley under neutral and unstable thermal stratifications. Four case studies, three of which pertain to unstable conditions, are presented to show the effects of thermal stratification, wind angle, and valley geometry on flow at bulk Richardson numbers near zero.

The numerical results discussed include the channeling of flow by the valley and the distribution of surface shear stress and heat flux. Occurring under neutral conditions as well as unstable ones, channeling is a dynamical phenomenon. A smaller amount of channeling takes place under unstable conditions, with valleys of larger aspect ratio, and in flows whose incoming surface winds make angles in the vicinity of 0° or 90° with the valley axis. The distributions of surface shear stress and heat flux feature two local maxima at the two outer corners of the valley and two local minima at the two corners of the valley floor. The effects on these distributions caused by varying the model parameters are also noted. Results are in excellent qualitative agreement with Taylor's results for flow over a valley under neutral conditions and, in a comparative neutral case study, in good quantitative agreement. The present work, however, being concerned largely with flows under unstable stratifications, is a considerable extension of Taylor's paper, which neglects the energy equation since only neutral conditions are considered.

1. Introduction

The gross features of the planetary boundary layer over flat terrain are reasonably well-understood, the fluid motion being determined by the large-scale pressure-gradient, Coriolis, and frictional forces. However, much of the earth is not flat, with a large portion of the population, industry and agriculture concentrated within valleys. Over such terrain atmospheric circulation is greatly modified and the flow patterns less understood. The study of valley meteorology is therefore a worthwhile pursuit.

A wide variety of flows within valleys have been observed and documented, e.g., Hewson and Gill (1944), Defant (1951). With light geostrophic winds, upvalley and upslope winds usually form during the day due to surface heating; at night, surface cooling commonly leads to drainage flows in the reverse directions. In addition, with differential solar heating of the valley slopes, a cross-valley wind component may also develop. On days with stronger synoptic flow, however, the streamlines deform to follow the valley shape, with slope winds being less important. Within the valley, channeling of the ambient wind toward a direction more nearly parallel to the valley axis is known to occur. In some cases, flow separation may occur over the windward slope.

There have been a sizeable number of analytical and numerical studies dealing with valley meteorology under conditions of no ambient wind. In this category the phenomena modeled are those arising from purely thermal effects—slope winds, moun-

[1] Present affiliation: Agricultural Weather Service Office, Department of Entomology, Michigan State University, East Lansing, Michigan 48824, USA.

tain-valley winds, and cross-valley winds. In contrast, there are surprisingly few studies in the journal literature dealing with valley meteorology under conditions of a prevailing synoptic flow. Representative are studies by Tang (1976), Taylor (1977a, b), and Bell and Thompson (1980).

Tang developed a linear analytical model to investigate the interaction between the thermal stratification and large-scale flow across a shallow sinusoidal valley. A region of reversed flow was found off the windward slope during the day and off the lee slope at night. Tang's model is limited through his assumption of periodic topography, his use of a constant eddy viscosity and neglect of horizontal transport of momentum and heat, and his omission of the axial velocity component and Coriolis forces.

Taylor (1977b) studied three-dimensional flow over a Gaussian valley under neutral stratification. His results on the channeling phenomenon indicate a greater amount of deflection in the surface wind for incoming flow at angles about $\pm 40°$ to the normal of the valley axis. Taylor's results also show a surface shear-stress distribution featuring two local maxima at the outer edges of the valley and a minimum just to the windward side of the trough. In his earlier paper, Taylor (1977a) investigated two-dimensional surface flow over a valley.

Bell and Thompson studied the interaction of strong stable stratification with a prevailing flow across a valley. They found no stagnant or reversed flow regions within the valley whenever their Froude number exceeded 1.3. Their numerical model, however, suffers from their assumption of no friction and use of periodic topography. Only two-dimensional flow is modeled and the mesh sizes used in the calculations are extremely coarse.

The present paper describes a numerical model designed to calculate the steady-state distributions of wind and temperature for flow over a valley. Two types of thermal stratification are modeled: (1) neutral and (2) unstable. In the latter case the assumption of a steady lower boundary layer under unstable conditions is based on observational evidence (Carlson, 1982). Typically, a sunny day features a one- or two-hour period in mid-afternoon when the vertical temperature profile in the lower boundary layer is quasi-steady. During unstable stratifications, then, the model is designed to simulate mid-afternoon conditions in the lower region of the boundary layer, a region which is assumed to be well below the capping stable layer and well within the mixed layer. To allow for steady-state conditions, the thermal boundary conditions are made sufficiently general to prevent a net accumulation of heat over time in this region.

The bulk Richardson number for the present problem indicates the relative importance of thermal effects to dynamic effects. In cases with bulk Richardson numbers near zero, the dynamic interactions of the flow with the valley will dominate. Four such case studies are presented in this paper to show the effect on the flow of thermal stratification, geostrophic wind angle, and valley geometry. In another paper (Carlson and Foster, 1985) case studies with bulk Richardson numbers in the vicinity of -1 (i.e. of order unity) are presented. In such flows, themal effects become important.

2. Governing equations

Consider first the geometric orientation of the valley for the present problem (Fig. 1). For a valley situated at latitude ϕ in the northern hemisphere, align the y-axis of a right-handed Cartesian coordinate system with the valley axis. Let the x-axis be in the cross-valley direction and the z-axis in the vertical. For mathematical simplicity the valley dimensions are considered invariant in the y direction (along its axis). If, in addition, it is assumed that the geostrophic wind and latitude ϕ do not vary over the region of concern, then any

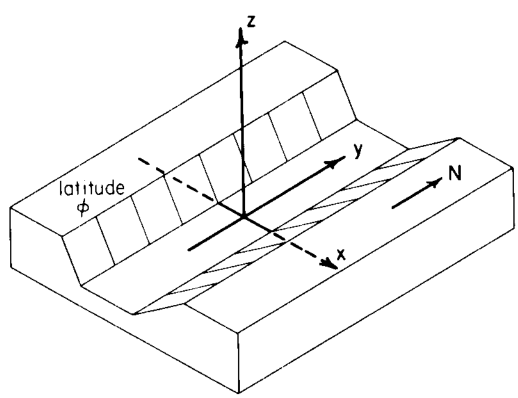

Fig. 1. Cartesian coordinate system for a valley at latitude ϕ in the northern hemisphere. Valley dimensions are invariant along the y-axis, which is directed northward for simplicity.

mathematical solution will be solely a function of x and z. For convenience in referencing wind direction, the valley axis is taken to be northward.

The atmospheric variables of pressure p, density ρ, and potential temperature θ are expressed as follows:

$$p(x, y, z, t) = p_0 + p_e(z) + p'(x, z, t) - \rho_0 f u_g y, \quad (1)$$

$$\rho(x, z, t) = \rho_0 + \rho_e(z) + \rho'(x, z, t), \quad (2)$$

$$\theta(x, z, t) = \theta_0 + \theta'(x, z, t). \quad (3)$$

Here p_0 is the surface ($z = 0$) value of p, and p_e, the vertical variation, all in an equilibrium adiabatic reference state (flat land, no motion). The variable p' is the perturbation from the reference state due to motion, valley topography, and time-dependent processes. The same definitions hold for the other two variables. To allow for a geostrophic wind component, u_g, in the x direction, the pressure field p varies linearly in the y direction; p', however, remains a function solely of x and z, as do all perturbations. The time variable is t and f is the Coriolis parameter.

First, the Boussinesq approximations (Spiegel and Veronis, 1960; Calder, 1968) are applied to the continuity equation, the thermal energy equation (no radiation sources assumed), and the Navier–Stokes equations for flow in a rotating system. Then, the Reynolds decomposition for turbulent flow variables is introduced (Busch, 1973) and the equations are averaged.

Next, we represent the Reynolds stresses and turbulent heat fluxes in terms of eddy exchange coefficients in the standard way:

$$\overline{u_i' u_j'} - \tfrac{1}{3} q^2 \delta_{ij} = -2K_m D_{ij} \quad (4)$$

$$\overline{\theta'' u_i'} = -K_h \partial \theta' / \partial x_i, \quad (5)$$

where

$$D_{ij} = \tfrac{1}{2}(\partial \bar{u}_i / \partial x_j + \partial \bar{u}_j / \partial x_i) \quad (6)$$

is the deformation tensor and $q^2 = (\overline{u_1'^2} + \overline{u_2'^2} + \overline{u_3'^2})$ is twice the turbulent kinetic energy. In addition, $\bar{u}_i$ denotes the mean value of the wind component in the x_i direction ($x_1 = x$, $x_2 = y$, $x_3 = z$); $\bar{\theta}'$, the mean value of potential temperature perturbation θ'; u_i' and θ'', the turbulent fluctuations about $\bar{u}_i$ and $\bar{\theta}'$, respectively; and K_m and K_h, the eddy viscosity and diffusivity, respectively. The particular way in which we model the dependence of K_m and K_h on the turbulence is discussed in Section 3.

Substituting (4) and (5) into the averaged equations and neglecting molecular viscosity and diffusivity, one arrives at the following five equations describing the mean flow:

$$\partial \bar{u}/\partial x + \partial \bar{w}/\partial z = 0, \quad (7)$$

$$\mathrm{D}\bar{u}/\mathrm{D}t = -(1/\rho_0)\, \partial \hat{p}/\partial x + f\bar{v} - 2\Omega\, \bar{w} \cos \phi + (\partial/\partial x)(2K_m\, \partial \bar{u}/\partial x) + (\partial/\partial z) \times [K_m(\partial \bar{u}/\partial z + \partial \bar{w}/\partial x)], \quad (8)$$

$$\mathrm{D}\bar{v}/\mathrm{D}t = f u_g - f\bar{u} + (\partial/\partial x)(K_m\, \partial \bar{v}/\partial x) + (\partial/\partial z) \times (K_m\, \partial \bar{v}/\partial z). \quad (9)$$

$$\mathrm{D}\bar{w}/\mathrm{D}t = -(1/\rho_0)\, \partial \hat{p}/\partial z + g\bar{\theta}'/\theta_0 + 2\Omega \bar{u} \cos \phi + (\partial/\partial x)[K_m(\partial \bar{u}/\partial z + \partial \bar{w}/\partial x)] + (\partial/\partial z) \times (2K_m\, \partial \bar{w}/\partial z), \quad (10)$$

$$\mathrm{D}\bar{\theta}'/\mathrm{D}t = (\partial/\partial x)(K_h\, \partial \bar{\theta}'/\partial x) + (\partial/\partial z) \times (K_h\, \partial \bar{\theta}'/\partial z), \quad (11)$$

where

$$\mathrm{D}/\mathrm{D}t = \partial/\partial t + \bar{u}(\partial/\partial x) + \bar{w}(\partial/\partial z) \quad (12)$$

and

$$\hat{p} = \bar{p}' + \tfrac{1}{3} q^2. \quad (13)$$

Here, $\bar{u}$, $\bar{v}$, and $\bar{w}$ are the mean flow components in the x, y, and z directions, respectively; Ω is the angular frequency of earth's rotation; and g is the gravitational acceleration.

One can reduce the set of five equations (7)–(11) to a set of four by introducing the streamfunction ψ and the vorticity component ξ about the y-axis:

$$\partial \psi/\partial z = \bar{u}, \qquad \partial \psi/\partial x = -\bar{w}, \quad (14)$$

$$\xi = \partial \bar{u}/\partial z - \partial \bar{w}/\partial x. \quad (15)$$

With these definitions and dropping the ($^-$) notation, one can reduce (7)–(11) to the following set:

$$\nabla^2 \psi = \xi, \quad (16)$$

$$\mathrm{D}\xi/\mathrm{D}t = -(g/\theta_0)\, \partial \theta'/\partial x + f(\partial v/\partial z) + \nabla^2(K_m \xi) + 2(\partial^2/\partial z^2)(K_m\, \partial w/\partial x) - 2(\partial^2/\partial x^2) \times (K_m\, \partial u/\partial z) - 4(\partial/\partial x)(\partial/\partial z)(K_m\, \partial w/\partial z), \quad (17)$$

$$\mathrm{D}v/\mathrm{D}t = f(u_g - u) + (\partial/\partial x)(K_m\, \partial v/\partial x) + (\partial/\partial z)(K_m\, \partial v/\partial z), \quad (18)$$

$$D\theta'/Dt = (\partial/\partial x)(K_h\, \partial\theta'/\partial x) + (\partial/\partial z) \times (K_h\, \partial\theta'/\partial z), \tag{19}$$

where

$$\nabla^2 = \partial^2/\partial x^2 + \partial^2/\partial z^2. \tag{20}$$

Hence, the pressure variable $\hat{p}$ is differentiated out and one need no longer consider either $\bar{p}'$ or q^2.

3. Turbulence model

Since (16)–(19) are used to describe the fluid dynamics of the present problem, the question of turbulence modeling here reduces to the question of what form the eddy viscosity K_m and diffusivity K_h are to take.

In this study we use a Prandtl mixing-length model for the eddy viscosity and diffusivity, and write

$$K_m = 2l_m^2(D_{ij}:D_{ij})^{1/2}, \tag{21}$$

$$K_h = 2l_h^2(D_{ij}:D_{ij})^{1/2}, \tag{22}$$

where D_{ij} is defined in (6) and l_m and l_h are the length scales of the energy-containing eddies.

In order to include flows under unstable thermal stratifications, the expressions for l_m and l_h should take into account both mechanically and thermally generated turbulence. For a stability parameter we use the dimensionless height ζ,

$$\zeta = z^*/L, \tag{23}$$

where z^* is the distance to the surface and L is the Monin–Obukhov length (Obukhov, 1946) defined by

$$L = -\rho_0 c_p \theta_0 u_*^3/kgQ. \tag{24}$$

Here c_p is the specific heat capacity of air at constant pressure; k, the von Karman constant; u_*, the surface friction velocity, which is the square root of the ratio of surface stress, τ, to density; and Q is the surface heat flux.

Scaling relationships in the constant-flux surface layer (Busch, 1973) together with the definitions of K_m and K_h, (21)–(22), lead to the following forms for l_m and l_h in this layer:

$$l_m = k(z^* + z_0)/\phi_m(\zeta), \tag{25}$$

$$l_h = k(z^* + z_0)/[\phi_m(\zeta)\phi_h(\zeta)]^{1/2}, \tag{26}$$

where ϕ_m and ϕ_h represent the functions for nondimensional wind shear and temperature gradient, respectively, and z_0 is the roughness length of the surface. The $(z^* + z_0)$ formulation has been chosen so that wind speed, in the explicit expression for wind speed in this layer (Businger, 1973), will go to zero at $z^* = 0$.

Blackadar (1962) introduced an expression for mixing length under neutral conditions which allows l to behave as kz^* near the surface (as it should in the log layer) and to approach a constant λ at the upper reaches of the planetary boundary layer. The present mixing lengths follow the general form of Blackadar's expression but differ in the following important ways: (1) diabatic conditions are permitted through the use of the ϕ_m and ϕ_h functions, (2) the mixing lengths retain their surface layer forms within a height δ^* above the surface, and (3) the expressions for l are piece-wise continuous in z^* and allow for a smooth transition at δ^* through the $(z^* - \delta^*)$ term in the denominators. The mixing lengths are specified as:

$$l_m = \begin{cases} \dfrac{k(z^* + z_0)/\phi_m(\zeta)}{1 + \{k(z^* - \delta^*)/(\lambda\phi_m(\zeta))\}} & \text{for } z^* > \delta^*, \\ k(z^* + z_0)/\phi_m(\zeta) & \text{for } z^* \leqslant \delta^*, \end{cases} \tag{27}$$

$$l_h = \begin{cases} \dfrac{k(z^* + z_0)/[\phi_m(\zeta)\,\phi_h(\zeta)]^{1/2}}{1 + \{k(z^* - \delta^*)/[\lambda(\phi_m(\zeta)\,\phi_h(\zeta))^{1/2}]\}} & \text{for } z^* > \delta^* \\ k(z^* + z_0)/[\phi_m(\zeta)\,\phi_h(\zeta)]^{1/2} & \text{for } z^* \leqslant \delta^*. \end{cases} \tag{28}$$

Here, λ is taken (Wu, 1965) as 30 m under neutral conditions and 100 m under unstable conditions. Again the $(z^* + z_0)$ formulation is used. Currently, δ^* is set to 2δ in the model, where δ is the surface layer depth explicitly modeled (see Subsection 4.1).

Finally, the forms chosen for the ϕ_m and ϕ_h functions are based on Dyer and Hick's (1970) work and are those recommended by Dyer (1974) in his review article:

$$\phi_m(\zeta) = (1 - 16\zeta)^{-1/4}, \qquad \text{for } \zeta \leqslant 0, \tag{29}$$

$$\phi_h(\zeta) = (1 - 16\zeta)^{-1/2}, \qquad \text{for } \zeta \leqslant 0. \tag{30}$$

In summary, the turbulence model in the present study involves the use of eddy viscosities K_m and diffusivities K_h modeled as (21) and (22), with l_m and l_h given by (27) and (28), respectively.

4. Formulation of the boundary-value problem

4.1. Description

First, consider the geometric configuration. Fig. 2 depicts the cross section of the valley in the x–z plane. As mentioned earlier, the valley dimensions are invariant in the y direction.

The region enclosed by the heavily shaded solid-line segments represents the domain of calculation. The left vertical segment is the inflow boundary and the right vertical segment, the outflow boundary. The series of segments at the bottom represent the contour of the valley surface S. They depict the two ridge surfaces of horizontal length X_r, the two sloped surfaces of horizontal extent X_s, and the valley floor width W. The valley has a depth H with slopes of angle α to the x-axis. The upper solid segment (at $z = z_t$) is the upper boundary of the domain and is a distance ($4H + \delta$) above the ridge surface. The region of thickness δ lying above the valley surface represents a layer within which temperature and wind profiles are modeled explicitly according to flux-profile relationships in the surface layer (Busch, 1973; Businger, 1973).

The upper boundary is at a level dividing two vertical regions. The lower region is the domain of calculation and is a region of three-dimensional flow and variable K_m and K_h. The upper region is a constant K_m Ekman layer with only horizontal flow. The top of this region is the top of the planetary boundary layer. We discuss the justification for two such regions in Subsection 4.3.

It should be mentioned that the model geometry shown in Fig. 2 as well as the upper ξ and v boundary conditions (to be later discussed) were designed to be appropriate for the valleys under study. Thus, $\delta = 0.125\ H$, for our choice of H (125 m), is a suitable surface layer depth, 16.5 m. If we had varied H greatly, a constant value for δ would have been the proper choice. Also, height z_t is assumed to be well below the capping stable layer during midday, yet well above the surface layer depth δ. Under these assumptions, $z_t = 5H + \delta$ is an appropriate choice. If H were to vary greatly, a different formulation for z_t and/or different upper ξ and v boundary conditions would have to be invoked.

Any specific problem of interest involves the specification of the geometrical parameters H, W, and α, as well as the following meteorological

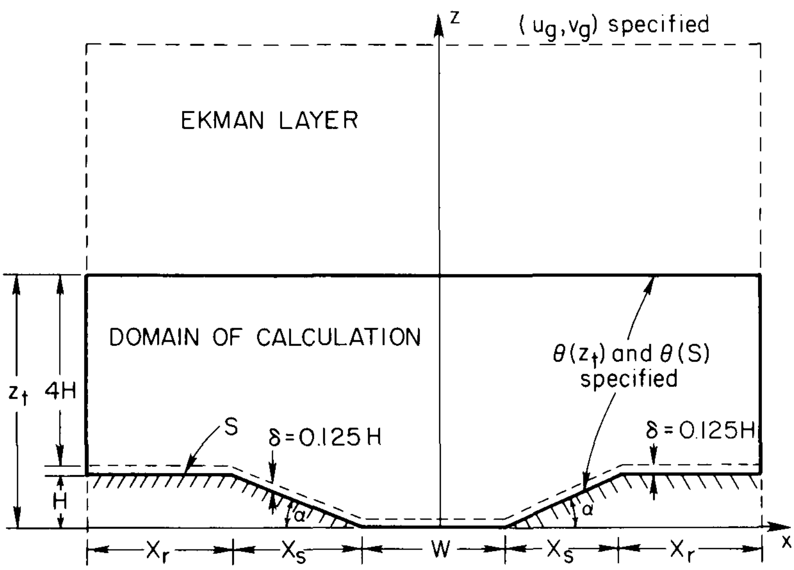

Fig. 2. The geometric configuration for the present problem. The independent parameters are u_g, v_g, $\theta(z_t)$, θ(S), H, W, and α.

parameters: (1) the geostrophic wind (u_g, v_g), (2) the potential temperature at $z = z_t$, and (3) the potential temperature distribution along S. The problem is then to seek a steady-state flow solution to (16)–(19).

4.2. *Special treatment of variables over non-horizontal terrain*

Because the mixing lengths (27) and (28) are to be used over non-horizontal terrain, the present model defines the z^* variable in the $k(z^* + z_0)$ terms as the shortest distance to the surface, since these terms are related to the mechanical production of turbulence. All other z^* variables, including those in the buoyancy-related ζ terms, represent the vertical distance to the surface. Taylor (1977a, b) uses a similar approach in his expression for l.

With respect to the equations describing the δ surface layer (Carlson, 1982), the gradients in wind speed and temperature are deemed normal to the surface as are all other variables in those equations except z^* in the ζ variable. In that variable, the surface heat flux Q in the expression for the Monin-Obukhov length (24) is defined as the vertical heat flux, since L appertains to buoyancy, which acts in the vertical.

4.3. *Boundary conditions*

The left inflow boundary presupposes that the flow has been traveling over horizontal terrain and hence is uniform in the x direction. These steady upstream profiles, u_L, v_L, and θ'_L are determined from a solution of (8), (9), and (11) with x and t derivatives of u, v, and θ' set to zero and $w = 0$ (Carlson, 1982). At the inflow boundary, then $\xi = \partial u_L/\partial z$, v, and θ' are specified from the upstream profiles, and $\partial\psi/\partial x = 0$.

The top boundary of the calculation is at $z = z_t$, which we assume to be high enough that w is negligible. If, in addition, barotropic conditions ($\partial\theta'/\partial x = 0$) exist above z_t, then the usual Ekman layer solution is, in fact, an exact solution to (7)–(11) for K_m and K_h constant, provided $\partial u/\partial x$ and $\partial v/\partial x$ are negligible there. A study one of us (JDC) conducted using 1979 data from the Tennessee Valley Authority showed that, for mid-day situations over a 275 m deep valley in Alabama, the temperature over the ridge and that over the valley were equal by an elevation, on the average, of 950 m. Hence, at a height of 2.5 H above the ridge, θ' was indeed x-independent. In addition, our numerical solutions show *a posteriori* the legitimacy of our assumptions: near the top of the domain, θ' (Fig. 10a), u (Fig. 5), and v (Fig. 6) are nearly x-independent. With such being the case, an Ekman spiral is the only appropriate solution for large distances above the valley. Any lesser, *ad hoc* boundary condition is incorrect. Finally, even under unstable stratifications, Ekman spirals have been shown to exist both observationally (Zilitinkevich et al., 1967) and theoretically (Yamamoto et al., 1968).

At $z = z_t$, then w is set to zero and θ' is set to a prescribed constant. Now $w = 0$ implies ψ is constant along the top. This ψ value is obtained through vertical integration of the u_L profile. To arrive at the ξ and v boundary conditions, we demand that the computed solution in $z < z_t$ for u, v, $\partial u/\partial z$, $\partial v/\partial z$, and K_m agree at $z = z_t$ with the analytical Ekman solution in $z > z_t$ (here, K_m scales with fU_g). That joining of the two solutions at $z = z_t$ leads to (Carlson, 1982):

$$\xi(x) = 2^{-1/2} f^{1/3}\, l_t(x)^{-2/3} \times (u_g - u_t(x) + v_t(x) - v_g)/[(u_g - u_t(x))^2 + (v_t(x) - v_g)^2]^{1/6}, \tag{31}$$

$$\partial v(x)/\partial z = 2^{-1/2} f^{1/3}\, l_t(x)^{-2/3}(u_g - u_t(x) + v_g - v_t(x))/[(u_g - u_t(x))^2 + (v_t(x) - v_g)^2]^{1/6}, \tag{32}$$

where l_t, u_t, and v_t denote the corresponding values of l_m, u, and v at the top of the domain.

The matter of the location of z_t is not a simple one. We have chosen 5H above the valley floor δ surface layer. One could argue that z_t should be larger, but to use a multiple of valley width, for example, would place the top of the domain of calculation, for cases 1–3, at about 1050 m for one such width and at about 2075 m for two widths. Such heights do not meet the criterion that z_t be sufficiently below the capping stable layer, which is typically situated around 1000 to 2000 m during mid-afternoon. More will be said about the choice of z_t, from a computational point of view, in Subsection 5.4.

Because of the valley influence on downstream flow, the upwind equilibrium profiles are not applied as boundary conditions at the right vertical boundary. This boundary, however, is assumed sufficiently downstream so that x-independence of the profiles is a good approximation. Accordingly, the x-derivatives of ξ, v, and θ' are set to zero and $\partial^2 \psi/\partial z^2 = \xi$, i.e., $\partial w/\partial x = 0$ at that boundary. In any case, we determined in the course of the research that the effect of varying the outflow boundary conditions is to produce only small changes in the vicinity of that boundary.

The valley surface S in the present model lies a distance z_0 above the true physical surface. Along S, ψ is set to zero to ensure no perpendicular flow, a no-slip condition on velocity is indirectly applied through use of an explicit expression for wind speed (Businger, 1973), and θ' is specified. Due to the large truncation errors which would otherwise arise near S in the numerical solution of this problem, the explicitly modeled surface layer mentioned earlier is employed. Because of this layer, conditions along S must be applied indirectly through boundary conditions at the top of this layer. ψ is found through integration of the theoretical u profile in a direction perpendicular to S. Conditions on ξ, v, and θ' result from surface-layer expressions (Carlson, 1982).

4.4. Non-dimensionalization

Let H be chosen as the characteristic length scale in the present problem, $U_g = (u_g^2 + v_g^2)^{1/2}$, the characteristic velocity scale, and $\Delta\theta$, the characteristic temperature scale, where $\Delta\theta$ represents the maximum difference in θ between $z = z_t$ and surfaces S. $\Delta\theta$ is always taken as non-negative. Then $u = \tilde{u}U_g$, $v = \tilde{v}U_g$, $w = \tilde{w}U_g$, $x = \tilde{x}H$, $z = \tilde{z}H$, $\theta' = \tilde{\theta}'\Delta\theta$, $t = \tilde{t}H/U_g$, $\xi = \tilde{\xi}U_g/H$, $\psi = \tilde{\psi}HU_g$, $K_m = \tilde{K}_m HU_g$, and $K_h = \tilde{K}_h HU_g$. Here quantities with tildes are the nondimensional forms. Substituting these dimensionless variables into (16)–(19) and dropping the ($\tilde{\ }$) notation, one obtains the governing equations in dimensionless form:

$$\nabla^2 \psi = \xi, \tag{33}$$

$$\begin{aligned} D\xi/Dt = {} & \mathrm{Ri_B}\, \partial\theta'/\partial x + (1/\mathrm{Ro})(\partial v/\partial z) \\ & + \nabla^2(K_m \xi) + 2(\partial^2/\partial z^2)(K_m \partial w/\partial x) \\ & - 2(\partial/\partial x^2)(K_m \partial u/\partial z) - 4(\partial/\partial x)(\partial/\partial z) \\ & \times (K_m \partial w/\partial z), \end{aligned} \tag{34}$$

$$\begin{aligned} Dv/Dt = {} & (1/\mathrm{Ro})(u_g/U_g - u) + (\partial/\partial x) \\ & \times (K_m \partial v/\partial x) + (\partial/\partial z)(K_m \partial v/\partial z), \end{aligned} \tag{35}$$

$$\begin{aligned} D\theta'/Dt = {} & (\partial/\partial x)(K_h \partial\theta'/\partial x) + (\partial/\partial z) \\ & \times (K_h \partial\theta'/\partial z). \end{aligned} \tag{36}$$

In (34) and (35) appear two nondimensional numbers, a bulk Richardson number ($\mathrm{Ri_B}$) and the Rossby number (Ro), where

$$\mathrm{Ri_B} = -gH\Delta\theta/U_g^2\,\theta_0, \tag{37}$$

$$\mathrm{Ro} = U_g/fH. \tag{38}$$

The bulk Richardson number is a measure of the baroclinic term to the inertia terms; the Rossby number, a measure of the importance of the inertia terms to the Coriolis terms.

5. Numerical formulation

5.1. Grid system and calculation sequence

The solution of the problem formulated in Section 4 is determined numerically over a two-dimensional, uniform rectangular grid. The lower boundary S is constrained to pass through the grid points and to have a slope of 0 of $\pm\Delta z/\Delta x$, where Δz and Δx are the nondimensional vertical and horizontal grid intervals respectively; i.e., $\Delta z/\Delta x = \tan\alpha$.

The steady-state solution of (34)–(37) is obtained by a simple methodology involving grid halving. Starting with general initial conditions, the unsteady u, v, and θ' equations are integrated in time (nondimensional time steps of Δt) over a coarse grid having $\Delta z = 0.5$ until the solution approaches a steady state. The next step is to halve the mesh spacing ($\Delta z = 0.25$). Using the interpolated results of the $\Delta z = 0.5$ calculation as initial conditions, the equations are again integrated in time until a steady state is neared. The procedure is repeated twice more. Hence, the final fine-grid solution is obtained on a grid with $\Delta z = 0.0625$ (16 vertical locations within the valley depth H).

For any given mesh size calculation, the advancement of the solution from time step n to $(n + 1)$ proceeds as depicted in Fig. 3. Eq. (34)–(36) are integrated over Δt and then (33) is solved for ψ^{n+1}. Since an implicit numerical method (to be later described) is used for the advancement of ξ, v, and θ' over time, the above procedure is repeated two times. Thereby, at the end of each iteration over Δt, the interior ψ^{n+1}, ξ^{n+1}, v^{n+1}, and $(\theta')^{n+1}$ are updated, as are their boundary values.

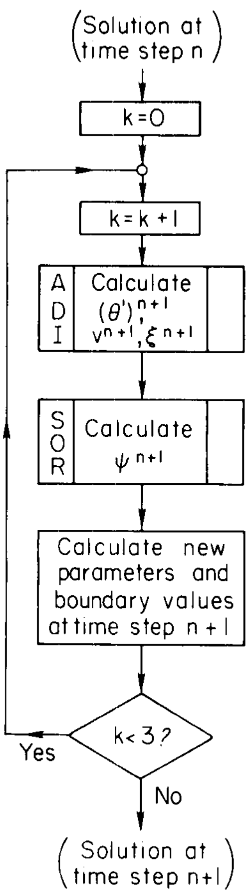

Fig. 3. Simplified flow chart for the advancement of the solution from time step n to $(n + 1)$.

5.2. *Finite differencing*

The governing equations (33)–(36) are written in finite-difference form, as are the boundary conditions. All spatial derivatives are at least second-order accurate in Δx and Δz. First-order forward differencing in time is used to advance over half a time step; over the entire time step, however, the differencing is second-order accurate in Δt (Carlson, 1982).

The spatial derivatives in (33)–(36) are all represented by central differences except in the case of the non-linear advective terms. Use of central differences in these terms led to flow oscillations or "parasitic" waves (Messinger and Arakawa, 1976). Such oscillations vanished when an "upwind" differencing algorithm was used. Second-order, three-point backward differencing into the wind is used. Upwind differencing should not be necessary for an unsteady elliptic problem; however, because of the boundary-layer character of the solutions, the equations are, in fact, nearly parabolic, and hence the downstream direction does become pseudo-time-like.*

Boundary conditions are expressed in terms of second- or third-order accurate differences; central differencing is used except where Neumann conditions make that impossible.

5.3. *Numerical methods*

The method of successive over-relaxation (SOR) is well-known (Roache, 1972; Ames, 1969) and is used to solve the Poisson equation, Eq. (33), at the end of each time step. A variation attributable to Sheldon (1960) is employed to solve the equation in "hopscotch" fashion. An over-relaxation constant of 1.7 was found to be an optimum value for the present problem. Iteration is terminated when

$$\max_{ij} \{ |\psi_{i,j}^{m+1} - \psi_{i,j}| / |\psi_{i,j}^{m+1}| \} < 10^{-2}, \tag{39}$$

where m is the iteration number and (i,j) denotes the location of the interior grid point.

The other three governing equations, (34)–(36), are solved by the alternating-direction implicit method (ADI). This method was introduced by Peaceman and Rachford (1955) and is discussed in Roache (1972) and Smith (1978). The Thomas algorithm is used along the x direction to advance the variables from time step n to $(n + \frac{1}{2})$; it is used along the z direction to advance the variables from $(n + \frac{1}{2})$ to $(n + 1)$.

An iterative numerical scheme is used to solve for the upstream u_L, v_L, and θ'_L profiles, which provide the basis for the inflow boundary conditions. The outflow boundary condition, $\partial^2\psi/\delta z^2 = \zeta$, is found using the Thomas algorithm again. The integrals used to compute the top and lower ψ conditions are evaluated by the trapezoidal rule.

5.4. *Accuracy*

All calculations were done in double-precision arithmetic on the Amdahl 470 V/6-II of The Ohio State University Instruction and Research Computer Center.

---

* Personal communication (1982) with O. R. Burggraf, Department of Aeronautical and Astronautical Engineering, The Ohio State University, Columbus, Ohio, U.S.A.

Table 1. *Richardson extrapolation of surface friction velocity* (u_*) *and heat flux* (Q) *results from case 2 at the four corners of the valley surface*

	$u_*(A)$[a] (m s^{-1})	$Q(A)$ (W m^{-2})	$u_*(B)$[b] (m s^{-1})	$Q(B)$ (W m^{-2})	$u_*(C)$[c] (m s^{-1})	$Q(C)$ (W m^{-2})	$u_*(D)$[d] (m s^{-1})	$Q(D)$ (W m^{-2})
Y_2 ($\Delta z = 0.125$)	0.55655	47.406	0.36036	29.936	0.37661	31.334	0.58545	49.395
Y_1 ($\Delta z = 0.0625$)	0.57180	49.135	0.36423	31.016	0.38055	32.411	0.60375	51.630
$Y_0(Y_2, Y_1)$	0.57690	49.713	0.36551	31.376	0.38187	32.771	0.60985	52.375
$\dfrac{\lvert Y_1 - Y_0(Y_2, Y_1)\rvert}{Y_1} (\times 10^2)$	0.89	1.18	0.35	1.16	0.35	1.11	1.01	1.44

[a] A—the windward upper corner.
[b] B—the windward lower corner.
[c] C—the leeward lower corner.
[d] D—the leeward upper corner.

Truncation error studies were performed (Appendix D of Carlson, 1982) in which Richardson extrapolation (Hildebrand, 1956) was applied to the $\Delta z = 0.125$ and $\Delta z = 0.0625$ converged calculations. The analysis was applied to the four governing variables at various interior grid points for a variety of case studies. Also, an analysis of the surface variables of friction velocity u_* and heat flux Q at the four corners of the valley surface was performed. Table 1 presents such an analysis for case 2 (see Section 6). Y_2 denotes the value at the $\Delta z = 0.0625$ mesh size, and Y_0 the "true" (zero mesh size) value. The last row contains the percentage truncation error associated with Y_1, the fine grid solution. These results, as do the others, show that the percentage errors are generally below 2%.

Difference tables (Hildebrand, 1956) were also constructed for the four governing variables at interior locations. The absolute magnitudes of the differences decrease from the first through the third difference for all variables except vorticity ξ near the valley surface, where at some locations the second difference exceeds the first. Clearly, a finer mesh spacing near the valley surface would have been desirable; computer memory limitations precluded that option. Nevertheless, as noted above, the accuracy of surface variable calculations is very good with the $\Delta z = 0.0625$ grid.

It would be naive to believe that the numerical results are independent of the geometrical domain of calculation (Fig. 2), i.e., independent of the height z_t chosen for the grid top above the valley floor and independent of the length X_r chosen for the ridge surfaces. Accordingly, studies were performed varying z_t and X_r. Grids top heights corresponding to $4H$, $5H$, and $6H$ $(+\delta)$ above the valley floor were chosen for the study. Results showed the percentage change in the solution to be much less in going from a top of $5H$ to $6H$ than from one of $4H$ to $5H$. For example, the changes in ψ and θ' at $z = 2H$ averaged 0.4% across the grid in going from a top of $5H$ to $6H$, while they averaged 1.2% in going from one of $4H$ to $5H$; the changes in surface variables u_* and Q averaged 0.8% versus 1.5%. Hence, $5H$ was chosen as a compromise. Also, lengths of $X_r = 2W$ ($X_r = 3W$ for case 4) were found to be sufficient to model homogeneous inflow near the left vertical boundary, as is postulated.

6. Results and discussion

Values of the input parameters used in our calculations are given in Table 2. Note that a valley

Table 2. *Values of the constant input parameters*

$k = 0.41$	$z_0 = 0.1$ m
$\rho_0 = 1.24$ kg m^{-3}	$\theta_0 = 300$ K
$c_p = 1.00 \times 10^3$ m^2 s^{-2} K^{-1}	$H = 125$ m
$g = 9.8$ m s^{-2}	$\alpha = 20°$
$f = 9.37 \times 10^{-5}$ s^{-1} ($\phi = 40°$)	

Table 3. *Parameter values in the four case studies*

Case	u_g (m s^{-1})	v_g (m s^{-1})	W/H	$\theta(z_t)$ (K)	θ(S) (K)	Ro	Ri_B
1	5	−10	2.75	300	300	955	0
2	5	−10	2.75	298.6	300	955	−0.0457
3	10	−5	2.75	298.6	300	955	−0.0457
4	5	−10	1.37	298.6	300	955	−0.0457

of slope 20° and depth 125 m was used at all times. These values are typical of valleys in the eastern United States. This particular choice for H results in a physical mesh size for the fine grid of $\Delta z = 7.8$ m and $\Delta x = 21.5$ m.

A total of nine case studies were performed. corresponding to different values of u_g, v_g, W/H, $\theta(z_t)$, and θ(S). These studies are fully described in Carlson (1982). Four of the numerical cases involving bulk Richardson numbers near zero are described in the present paper; cases involving bulk Richardson numbers of order one are given in Carlson and Foster (1985).

Table 3 presents the parameter values and resulting Rossby and bulk Richardson numbers for the four cases to be discussed. Cases 1 and 2 are identical except for the thermal stratification, case 1 being neutral. Case 3 differs from case 2 only in wind angle. Case 4 differs from case 2 only in aspect ratio, W/H. The numerically large values of the Rossby number arise from the definition incorporating the vertical scale H rather than the usual horizontal scale. In any case, Coriolis forces are not important in most of the domain. Their main rôles are in determining the equilibrium inflow wind spiral and allowing smooth transition to the Ekman spiral above z_t. The small Richardson numbers indicate that dynamic effects are more important than thermal effects in these cases. Additional cases for Ri_B of −0.0980 and −0.0245 may be found in Carlson (1982). The four cases presented here are chosen because they clearly indicate the effects of changing thermal stratification, wind angle, and aspect ratio.

6.1. Channeling

Fig. 4 presents a top view of the trajectories for two air parcels crossing the valley in case 1, the neutral case. Both air parcels are released at the left inflow boundary, but one is released at the top of the grid and the other within the surface layer of thickness δ. It is clear that strong channeling occurs near the surface. As the air parcel enters the valley region, it is deflected toward a direction more nearly parallel to the valley axis. At the top of the grid, little channeling is evident.

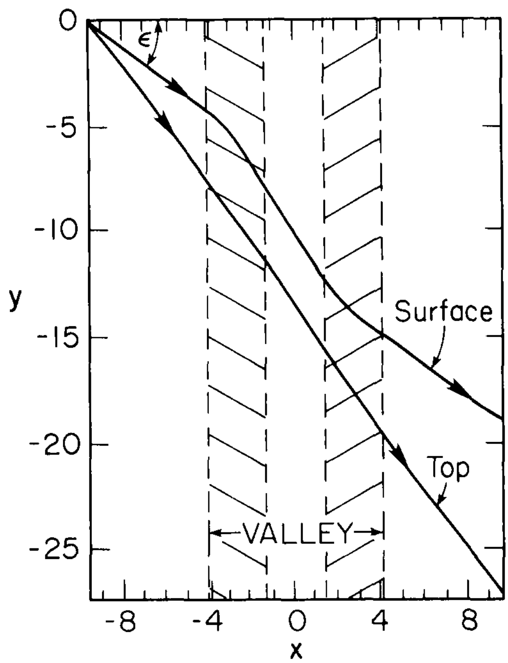

Fig. 4. Top view of air parcel trajectories for case 1. The angle of incidence of the incoming surface flow is ε. Length scales are dimensionless.

Channeling is clearly a dynamical phenomenon, occurring as it does under neutral stratification. Figs. 5 and 6 help explain its physical basis. In these, as in all contour plots, the vertical scale is exaggerated for greater clarity. Fig. 5 is a contour plot of the streamfunction ψ and shows the flow

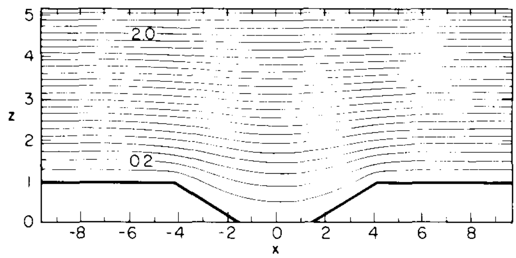

Fig. 5. Streamfunction (ψ) contours for case 1. The contour interval is 0.1. All values are non-dimensional.

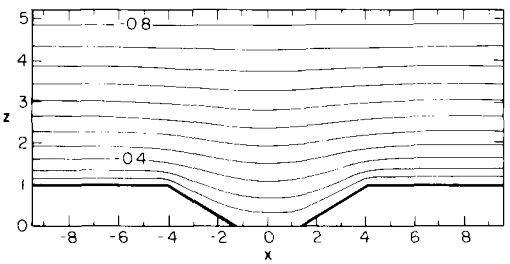

Fig. 6. Contour plot of v for case 1. The contour interval is 0.05, with isopleths below the $v = -0.3$ contour omitted. All values are non-dimensional.

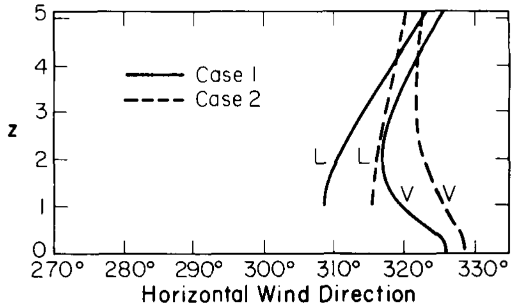

Fig. 7. Vertical profiles of horizontal wind direction at two surface locations for cases 1 and 2. L denotes the left inflow boundary and V, the centre of the valley floor. Height is dimensionless.

deformation over the valley. The normal distance between these lines is inversely proportional to the local magnitude of the wind component in the x–z plane. Fig. 6 is a contour plot of v, the y-velocity component. It is clear from the vertical spacing between streamlines in Fig. 5 that u, the x-velocity component, decreases as air descends into the valley. The fact is a consequence of the conservation of mass in airflow between the surface $S(\psi = 0)$ and grid top ($\psi =$ constant). Fig. 6 indicates that the v contours closely parallel the ψ contours, which means that v changes very little as the air traverses the valley. Hence, the relative decrease in the magnitude of v is much less than that in u as air descends into the valley, resulting in a turning of the wind vector, i.e., channeling.

Case 2 shows that less channeling occurs in an unstably stratified atmosphere than in a neutral one. Fig. 7 is a comparison plot of the vertical profiles of horizontal wind direction at two surface locations for cases 1 and 2. The letter L denotes those profiles at the left inflow boundary and V, those at the centre of the valley floor. The valley profiles show that the amount of channeling within the valley increases with decreasing distance to the surface. Clearly, case 2 exhibits less channeling than case 1. Note also the typical Ekman turning in the upper regions of the profiles.

The reason behind this decreased channeling can be seen through Fig. 8, which is a comparison plot of the vertical profiles of wind speed for these two cases. The greater amount of turbulent mixing which occurs in an unstable atmosphere causes a greater transfer of momentum toward the surface, resulting in greater speeds near the surface and lower speeds further up for case 2 in comparison with case 1. This greater momentum transport also manifests itself in a smaller backing of the wind with height in the upper regions and a smaller amount of channeling within the valley (Fig. 7).

With the aid of Table 4, which lists some numerical results from the four case studies, case 3 may be compared with case 2 to see the effect of incident wind angle. Case 3 has a surface wind direction at the left boundary (β_L) of 279°, giving nearly perpendicular flow to the valley axis. β_L for case 2 is 316°, a much more oblique angle to the valley axis. The channeling $\beta_V - \beta_L$, of 5.3° for case 3 is much less than that in case 2 (12.7°). Hence, channeling is clearly dependent on the angle of incidence ε of the incoming surface flow to the normal of the valley axis (see Fig. 4). From geometrical considerations, given a similar percentage reduction in u for any flow crossing the valley, the amount of channeling should be least for those flows having angles of incidence in the vicinity of 0° and 90°. This wind angle effect under unstable conditions is similar to Taylor's (1977b) results for flow under neutral conditions.

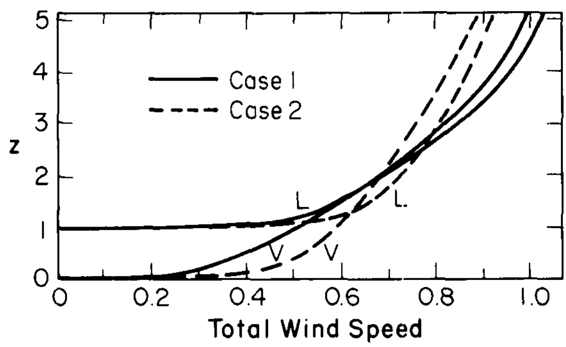

Fig. 8. Vertical profiles of total wind speed at two surface locations for cases 1 and 2. L denotes the left inflow boundary and V, the centre of the valley floor. All values are non-dimensional.

Table 4. *Some numerical results from the four case studies (L denotes the left inflow boundary and V the centre of the valley floor)*

Case	$\lvert u_L \rvert_\delta$ [a] (m s^{-1})	β_L [b] (deg)	$\beta_V - \beta_L$ (deg)	τ_L (N m^{-2})	τ_{max} (N m^{-2})	τ_{min} (N m^{-2})	Q_L [c] (W m^{-2})	Q_{max} (W m^{-2})	Q_{min} (W m^{-2})
1	5.18	308.8	17.3	0.218	0.323	0.067	0	0	0
2	6.04	315.8	12.7	0.320	0.452	0.165	44.75	51.61	31.02
3	6.03	278.9	5.3	0.319	0.601	0.074	44.66	61.66	25.20
4	6.05	315.7	16.7	0.321	0.445	0.161	44.79	51.36	30.64

[a] The wind speed at the top layer of the surface layer at the left boundary.
[b] β—the surface layer wind direction.
[c] Q—the heat flux normal to the surface.

Case 4 is identical to case 2 except in aspect ratio. Case 4 represents a narrower valley. Greater channeling occurs in this case (16.7°) because the smaller valley width restricts the amount of x-momentum which can be transported downward into the valley, resulting in lower u values there and, accordingly more channeling.

6.2. *Distributions of surface shear stress and heat flux*

Two calculated surface parameters of interest are the shear stress τ and heat flux Q. In all four cases the distributions of both quantities feature two local maxima at the two outer corners of the valley surface and two local minima at the two inner corners. Such a distribution is similar to that found by Taylor (1977b) for surface stress under neutral flow conditions. For each quantity the minimum at the windward inner corner has the smaller value of the two minima, and the maximum at the leeward outer corner, the greater value of the two maxima. Fig. 9a is a contour plot of vorticity ξ and Fig. 9b, a graph of shear stress versus x. Fig. 10a is a contour plot of perturbation potential temperature θ' and Fig. 10b, a graph of heat flux versus x. These graphs, taken from case 2, are typical of all four cases with the exception of case 1, which has no θ' or Q distribution.

Table 4 gives the entrance values of surface stress (τ_L) and heat flux (Q_L) as well as the maximum and minimum values of τ and Q for each case. As expected, the shear stress values are greater in case 2 than in case 1 due to the greater turbulent mixing. Case 3 has a surface flow angle nearly perpendicular to the valley axis. In such a case the dynamical influence of the valley on the flow is enhanced, since now most of the momentum is in the x direction. Accordingly, τ_{max} and Q_{max} are greater than their counterparts in case 2, and τ_{min} and Q_{min} are lower. This behavior, too, is in qualitative agreement with Taylor's (1977b) results

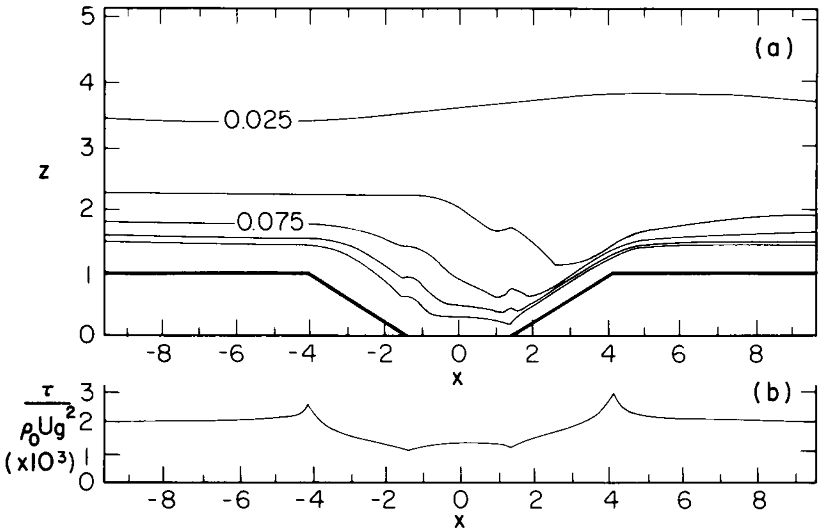

Fig. 9. (a) Vorticity (ξ) contours and (b) surface shear stress (τ) distribution for case 2. The contour interval for ξ is 0.025, with isopleths below the $\xi = 0.125$ contour omitted. All values are non-dimensional.

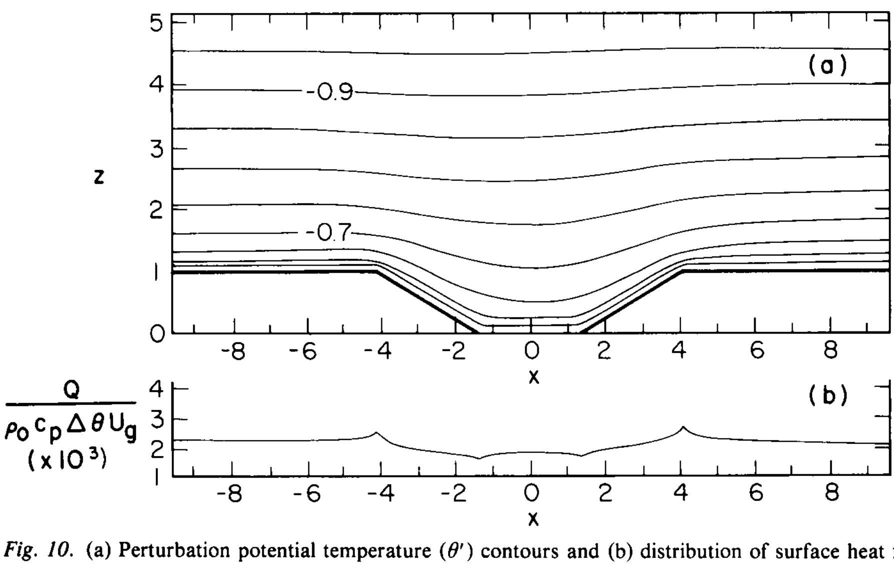

Fig. 10. (a) Perturbation potential temperature (θ') contours and (b) distribution of surface heat flux normal to the surface (Q) for case 2. The contour interval for θ' is 0.05, with isopleths below the $\theta' = -0.55$ contour omitted. $\theta' = 0$ at the valley surface. All values are non-dimensional.

for neutral flows. In case 4, τ_{max}, τ_{min}, Q_{max}, and Q_{min} are slightly lower than in case 2.

6.3. *Comparison with another numerical model*

To see how the valley model compares quantitatively with another such model, the authors, as nearly as possible, simulated with the present model the $\alpha_u = -45°$ calculation of Taylor's (1977b) model for neutral flow over a valley. A four-cornered valley with $H = 60$ m, $W = 200$ m, and $\alpha = 8.5°$ was used to approximate Taylor's Gaussian valley. With Taylor's use of 10^7 for the surface Rossby number, the values used in our computation were $u_g = 10$ m s^{-1}, $v_g = -10$ m s^{-1}, $z_0 = 1.51$ cm, $f = 9.37 \times 10^{-5}$ s^{-1}, and $\lambda = 60$ m.

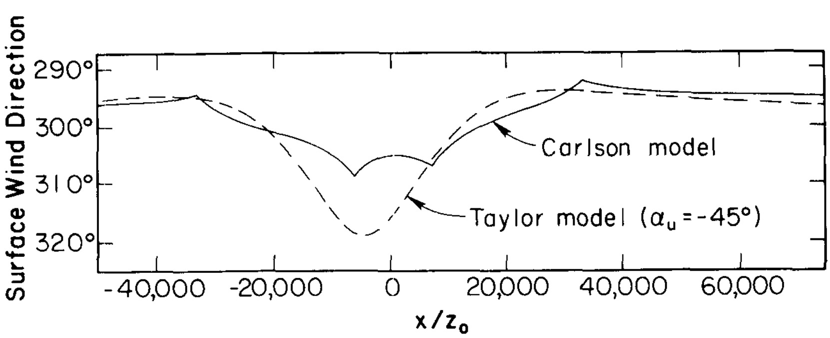

Fig. 11. Distributions of computed surface wind direction given by Taylor's (1977b) model and the present model. Here, x has been non-dimensionalized by the surface roughness z_0.

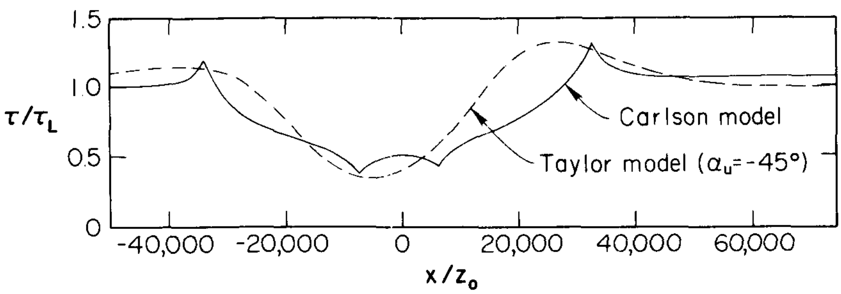

Fig. 12. Distributions of computed surface shear stress given by Taylor's (1977b) model and the present model. Here x has been non-dimensionalized by the surface roughness length z_0, and τ, by the surface stress at the left inflow boundary, τ_L.

First, consider the agreement between the wind profiles at the inflow boundary (i.e., over flat earth). Taylor predicts an 18.68° backing of the wind vector with height from the surface to the geostrophic level. The present model predicts an 18.24° backing. Taylor predicts a u_* of 0.459 m s^{-1}; the present model yields 0.472 m s^{-1}. Thus, excellent agreement is obtained over flat earth.

Next, consider Fig. 11, which depicts the surface wind direction over the valley surface given by the two models. The amount of channeling predicted by the present model is considerably less, the greatest discrepancy being about 10° at the valley floor. The explanation of this discrepancy appears to be twofold: (a) Taylor does not demand a log layer near the surface—he allows wind directions to change right down to the ground surface, and (b) our explicitly modeled surface layer appears to prematurely cut off the vertical changes in wind direction above the valley surface (Fig. 7); Thus, had a thinner surface layer been used, greater channeling probably would have resulted. Indeed, a thinner surface layer, one of nondimensional depth $\delta = 0.0625$, was tried in the course of the research, but very large truncation errors near the surface (associated with the computer-core limited mesh spacing of $\Delta z = 0.0625$) prevented its use.

Last, consider Fig. 12, which compares the surface shear-stress distributions given by the two models. Here the agreement is very good, with the local maxima and minima of the present model being of nearly equal value to those of Taylor's model. In both figures the cusps in the curves given by the present model are a result of using a valley with distinct corners.

7. Summary and conclusions

A two-dimensional numerical model has been developed to investigate steady-state, three-dimensional turbulent atmospheric flow over a valley under neutral and unstable thermal stratifications. The latter situation is representative of mid-afternoon conditions on a sunny day. The numerical model improves upon earlier models of flow over valleys by not assuming periodic topography, including Coriolis forces and the axial velocity component, allowing for unstable thermal stratification, and utilizing a moderately sophisticated model for eddy viscosity and diffusivity.

The four case studies presented in this paper appertain to flows having bulk Richardson numbers near zero, i.e., to flows where the dynamic effects of topography are more important than the thermal effects. The more salient conclusions which can be drawn from these studies are as follows.

(1) Channeling of flow by a valley is a dynamical phenomenon caused by a greater percentage decrease in the cross-valley component as compared to that in the axial component as air descends into the valley. The amount of channeling is strongly dependent on the angle of the incoming surface flow to the valley axis, being much less for angles of incidence near 0° and 90°. Channeling is also less under unstable thermal stratification (as compared to neutral) and with valleys of larger aspect ratio.

(2) The distributions of surface shear stress and heat flux feature two local maxima at the two outer corners of the valley surface and two local minima at the two corners of the valley floor. The stresses are greater under unstable conditions as compared to neutral. For flow of the same magnitude but with an angle of incidence closer to 0°, the maxima of both variables are greater and the minima smaller.

(3) No flow separation occurs within the range of conditions studied. A valley slope greater than the 20° used and higher ambient winds may be required before the onset of dynamical separation.

The numerical results are in excellent qualitative agreement with those of Taylor (1977b) for flow over a valley under neutral stratification. In addition, a comparative case study yielded good quantitative agreement. The present work, however, dealing largely with flows under unstable stratifications, constitutes a considerable addition to Taylor's paper.

8. Acknowledgments

The authors would like to thank Professors O. R. Burggraf and A. T. Conlisk for their interest and contributions during the course of this research. Numerical calculations were performed at The Ohio State University Instruction and Research Computer Center; special thanks to Mr. Michael Miller for his aid in obtaining sufficient funds for our computations. The preparation of this paper was supported in part by a grant from the Ohio Air Quality Development Authority (OSU Project Number 529629).

REFERENCES

Ames, W. 1969. *Numerical methods for partial differential equations*. New York, Barnes and Noble, 291 pp.

Bell, R. C. and Thompson, R. O. R. Y. 1980. Valley ventilation by cross winds. *J. Fluid Mech. 96*, 757–767.

Blackadar, A. K. 1962. The vertical distribution of wind and turbulent exchange in a neutral atmosphere. *J. Geophys. Res. 67*, 3095–3102.

Busch, N. E. 1973. On the mechanics of atmospheric turbulence. *Workshop on micrometeorology*, ed. D. A. Haugen. Boston, Amer. Meteorol. Soc., 1–65.

Businger, J. A. 1973. Turbulent transfer in the atmospheric surface layer. *Workshop on micrometeorology*, ed. D. A. Haugen. Boston, Amer. Meteorol. Soc., 67–100.

Calder, K. L. 1968. In clarification of the equations of shallow-layer thermal convection for a compressible fluid based on the Boussinesq approximation. *Q. J. R. Meteorol. Soc. 94*, 88–92.

Carlson, J. D. 1982. Numerical calculation of steady-state turbulent atmospheric flows over a valley under neutral and unstable thermal stratifications. Ph.D. dissertation, Atmospheric Sciences Program, The Ohio State University, Columbus, Ohio, 320 pp.

Carlson, J. D. and Foster, M. R. 1985. Numerical study of some unstably stratified boundary-layer flows over a valley at moderate Richardson number. *J. Clim. Appl. Meteorol.*, in press.

Defant, F. 1951. Local winds. *Compendium of meteorology*, ed. T. F. Malone. Boston, Amer. Meteorol. Soc., 655–672.

Dyer, A. J. 1974. A review of flux-profile relationships. *Bound.-Layer Meteorol. 7*, 363–372.

Dyer, A. J. and Hicks, B. B. 1970. Flux-gradient relationships in the constant flux layer. *Q. J. R. Meteorol. Soc. 96*, 715–721.

Hewson, E. W. and Gill, G. C. 1944. Meteorological investigations in Columbia River Valley near Trail, B. C. *Bur. of Mines Bull. 453*, 23–228.

Hildebrand, F. B. 1956. *Introduction to numerical analysis*. Toronto, McGraw-Hill, 511 pp.

Mesinger, F. and Arakawa, A. 1976. Numerical methods used in atmospheric models, Vol. I. GARP Publication Series No. 17, WMO-ICSU Joint Organizing Committee, 64 pp.

Obukhov, A. M. 1946. Turbulence in an atmosphere with a non-uniform temperature. *Tr. Inst. Teoret. Geofis. Akad. Nauk SSSR 1*, 95–111 (in Russian). Translation in *Bound.-Layer Meteorol. 2*, 7–29.

Peaceman, D. W. and Rachford, H. H. Jr. 1955. The numerical solution of parabolic and elliptic differential equations. *J. Soc. Indust. Appl. Math. 3*, 28–41.

Roache, P. J. 1972. *Computational fluid dynamics*. Albuquerque, New Mexico, Hermosa Publishers, 434 pp.

Sheldon, J. W. 1960. Iterative methods for the solution of elliptic partial differential equations. *Mathematical methods for digital computers*, eds. A. Ralston and H. S. Wilf. New York, John Wiley and Sons, 144–156.

Smith, G. D. 1978. *Numerical solution to partial differential equations: finite difference methods*. Oxford, Oxford Univ. Press, 299 pp.

Spiegel, E. A. and Veronis, G. 1960. On the Boussinesq approximation for a compressible fluid. *Astrophys. J. 131*, 442–447.

Tang, W. 1976. Theoretical study of cross-valley wind circulation. *Arch. Meteorol. Geophys. Bioklim. A25*, 1–18.

Taylor, P. A. 1977a. Some numerical studies of surface boundary-layer flow above gentle topography. *Bound.-Layer Meteorol. 11*, 439–465.

Taylor, P. A. 1977b. Numerical studies of neutrally stratified planetary boundary-layer flow above gentle topography. *Bound.-Layer Meteorol. 12*, 37–60.

Wu, S. 1965. A study of heat transfer coefficients in the lowest 400 m of the atmosphere. *J. Geophys. Res. 70*, 1801–1807.

Yamamoto, G., Yasuda, N. and Shimanuki, A. 1968. Effect of thermal stratification on the Ekman layer. *J. Meteorol. Soc. Japan 46*, 442–454.

Zilitinkevich, S., Laikhtman, D. and Monin, A. S. 1967. Dynamics of the atmospheric boundary layer. *Izv., Atmos. and Oceanic Phys. 3*, 297–333.